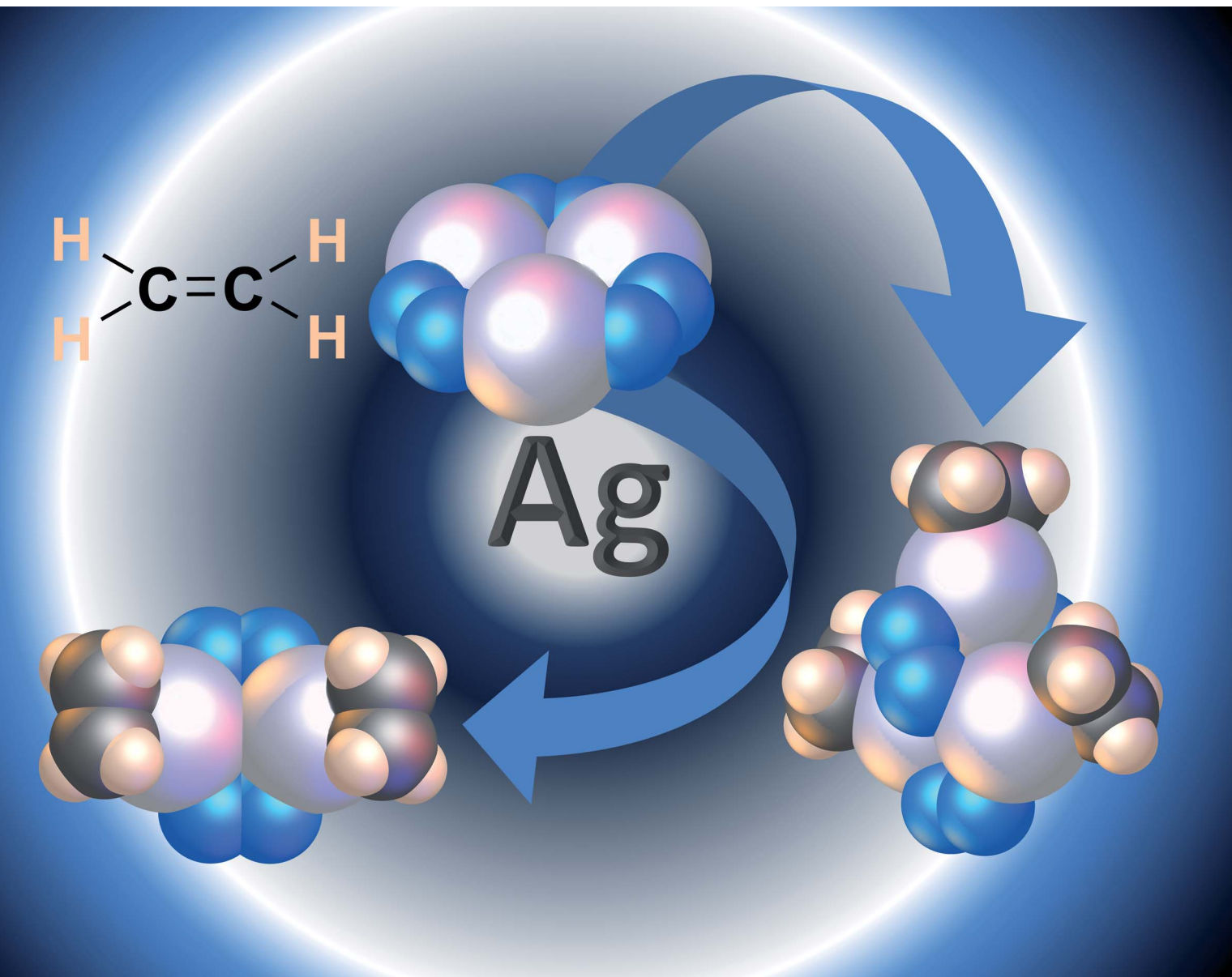


Chemical Science

rsc.li/chemical-science



ISSN 2041-6539

EDGE ARTICLE

H. V. Rasika Dias, Andrey A. Yakovenko, Peter W. Stephens,
Álvaro Muñoz-Castro *et al.*

In situ studies of reversible solid-gas reactions of ethylene
responsive silver pyrazolates

Cite this: *Chem. Sci.*, 2024, **15**, 2019

All publication charges for this article have been paid for by the Royal Society of Chemistry

Received 10th August 2023
Accepted 28th November 2023

DOI: 10.1039/d3sc04182d
rsc.li/chemical-science

Introduction

Trinuclear silver(i) complexes of fluorinated pyrazolates have attracted significant interest because many of them show interesting π -acid properties, luminescence, argentophilic contacts, and useful applications.^{1–8} For example, $\{[3,5-(CF_3)_2Pz]Ag\}_3$ (Fig. 1, $[\text{Ag-H}]_3$) reported by Dias *et al.*⁹ is a strong π -acid and displays rich π -acid/ π -base chemistry with unsaturated hydrocarbons leading to sandwich complexes of various types.¹⁰ It also serves as a sensor for arenes such as benzene and toluene.^{11,12} With *o*-terphenyl,¹³ it produces a white light emitting material while the treatment of $[\text{Ag-H}]_3$ with phenyl-acetylene produces a Ag_{13} cluster with the breakup of the Ag_3N_6

core.¹⁴ The silver complex has also been utilized in the desulfurization of fossil fuels.¹⁵

In contrast to the aromatic hydrocarbons, the chemistry of industrially relevant gaseous hydrocarbons such as ethylene with silver pyrazolates has not been explored. Silver–ethylene complexes are of particular interest since silver is the metal of choice for partial oxidation of ethylene, which is a major industrial process.^{16,17} They are challenging to stabilize and quite labile due to the relatively weak silver(i)–ethylene interactions.^{18–24} Reversible binding of ethylene to silver, however, is valuable in applications such as the separation of ethylene from ethylene–ethane mixtures using silver complexes

^aDepartment of Chemistry and Biochemistry, The University of Texas at Arlington, Arlington, Texas 76019, USA. E-mail: dias@uta.edu

^bX-Ray Science Division, Advanced Photon Source, Argonne National Laboratory, Argonne, Illinois 60439, USA. E-mail: ayakovenko@anl.gov

^cDepartment of Physics and Astronomy, Stony Brook University, Stony Brook, NY 11794-3800, USA. E-mail: peter.stephens@stonybrook.edu

^dFacultad de Ingeniería, Arquitectura y Diseño, Universidad San Sebastián, Bellavista 7, Santiago, 8420524, Chile. E-mail: alvaro.munozc@uss.cl

^eEnamine Ltd., Winston Churchill Street 78, 02094 Kyiv, Ukraine

^fTaras Shevchenko National University of Kyiv, Faculty of Chemistry, Volodymyrska 60, 01601 Kyiv, Ukraine

† Electronic supplementary information (ESI) available: Details of the synthesis of $[\text{Ag-CF}_3]_3$ and $[\text{Ag-CF}_3 \cdot (\text{C}_2\text{H}_4)]_2$ via solution methods, and the *in situ* solid phase synthesis of $[\text{Ag-CF}_3 \cdot (\text{C}_2\text{H}_4)]_2$, $[\text{Ag-H} \cdot (\text{C}_2\text{H}_4)]_3$ and $[\text{Ag-Br} \cdot (\text{C}_2\text{H}_4)]_2$, and the reverse processes, and molecular structure determinations using crystal X-ray crystallography and PXRD. Computational analysis of the ethylene uptake by silver pyrazolates, reaction pathways, additional figures, and references. CCDC 2256899, 2256900, 2266816–2266818 and 2267047. For ESI and crystallographic data in CIF or other electronic format see DOI: <https://doi.org/10.1039/d3sc04182d>

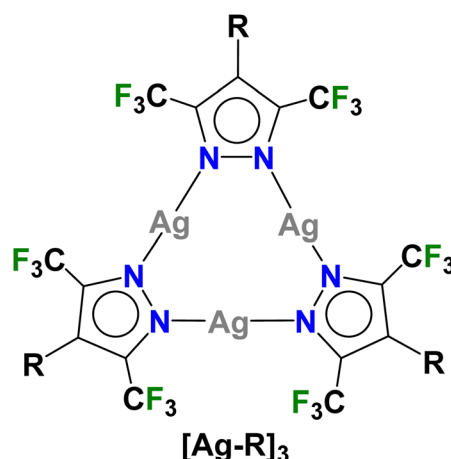


Fig. 1 Trinuclear silver(i)-pyrazolates utilized in this work, $\{[4-\text{R}-3,5-(CF_3)_2Pz]Ag\}_3$ ($[\text{Ag-R}]_3$, $\text{R} = \text{H}, \text{Br}, \text{CF}_3$).



and silver-doped materials.^{25–27} The copper(i) analogs of $[\text{Ag}-\text{H}]_3$ such as $\{[4-\text{R}-3,5-(\text{CF}_3)_2\text{Pz}]\text{Cu}\}_3$ ($[\text{Cu}-\text{R}]_3$, R = H, CF₃) are effective in the selective separation of ethylene from ethane containing mixtures.^{28,29}

Motivated by the fundamental interest and novelty, we embarked on an in-depth study of ethylene chemistry of silver(i) pyrazolates $\{[4-\text{R}-3,5-(\text{CF}_3)_2\text{Pz}]\text{Ag}\}_3$ ($[\text{Ag}-\text{R}]_3$, R = H, Br, CF₃) with different pyrazolyl ring substituents that also utilizes solid-gas^{30–33} synthesis and *in situ* powder X-ray diffraction (PXRD) measurements at 17-BM beamline at the Argonne National Laboratory (ANL) advanced photon source. As evident from the following account, this undertaking was successful and led to the stabilization of an unusual trinuclear silver–ethylene complex in a crystalline state. We also uncovered two unprecedented dinuclear silver–ethylene complexes with bridging pyrazolates, of which, only one could be obtained *via* a traditional solution method.

Results and discussion

Traditional solution chemistry

The per-fluorinated silver(i) complex $\{[3,4,5-(\text{CF}_3)_3\text{Pz}]\text{Ag}\}_3$ ($[\text{Ag}-\text{CF}_3]_3$) was utilized first for this purpose because it possesses powerful Lewis acidic silver sites and is expected to be more reactive towards ethylene compared to the less-fluorinated analogs. The $[\text{Ag}-\text{CF}_3]_3$ was obtained very conveniently *via* a reaction between the corresponding pyrazole $[3,4,5-(\text{CF}_3)_3\text{Pz}] \text{H}$ ³⁴ and silver(i) oxide. It is a colorless, air-stable solid and has been characterized by several techniques including NMR spectroscopy, and single crystal and powder X-ray crystallography. It crystallizes with a molecule of dichloromethane in the asymmetric unit (Fig. 2, see ESI for additional details and Fig. S7–S8†) and displays short intermolecular Ag···Cl and Ag···F contacts. There are no argentophilic interactions as observed in $[\text{Ag}-\text{H}]_3$ or electron-rich systems like $\{[3,5-(\text{Ph})_2\text{Pz}]\text{Ag}\}_3$ and $\{[3,5-(i\text{-Pr})_2\text{Pz}]\text{Ag}\}_3$.^{35–37}

More importantly, $[\text{Ag}-\text{CF}_3]_3$ reacts with ethylene in CH₂Cl₂ at low temperatures and produces a product which can be crystallized from the same mixture at –25 °C under an ethylene blanket (Scheme 1). The variable temperature ¹⁹F NMR spectroscopic data show that this transformation takes place below –10 °C in CDCl₃ (Fig. S4†). The analysis of crystalline solid using single crystal X-ray diffraction reveals that it is a dinuclear species $[\text{Ag}-\text{CF}_3 \cdot (\text{C}_2\text{H}_4)]_2$ (Fig. 2), and a rare isolable silver–ethylene complex.^{20,22,23,38–54} Solid samples, however, lose ethylene rapidly upon removal from the ethylene atmosphere at room temperature and return to the ethylene-free trimer form $[\text{Ag}-\text{CF}_3]_3$ (Scheme 1).

There are two chemically similar but crystallographically different molecules of $[\text{Ag}-\text{CF}_3 \cdot (\text{C}_2\text{H}_4)]_2$ in the asymmetric unit. The silver sites are trigonal planar and Ag₂N₄ cores adopt a boat shape. Although there are no analogous dinuclear silver–ethylene complexes for a direct comparison, a few silver–ethylene complexes such as $[\text{PhB}(3-(\text{CF}_3)\text{Pz})_3]\text{Ag}(\text{C}_2\text{H}_4)$ ⁴¹ and $\{[\text{H}_2\text{C}(3,5-(\text{CF}_3)_2\text{Pz})_2]\text{Ag}(\text{C}_2\text{H}_4)\}[\text{SbF}_6]$ ²⁰ with a three coordinate silver sites supported by N-donor ligands are known. The average Ag–N (2.231 Å) and Ag–C (2.282 Å) distances of $[\text{Ag}-\text{CF}_3]_3$

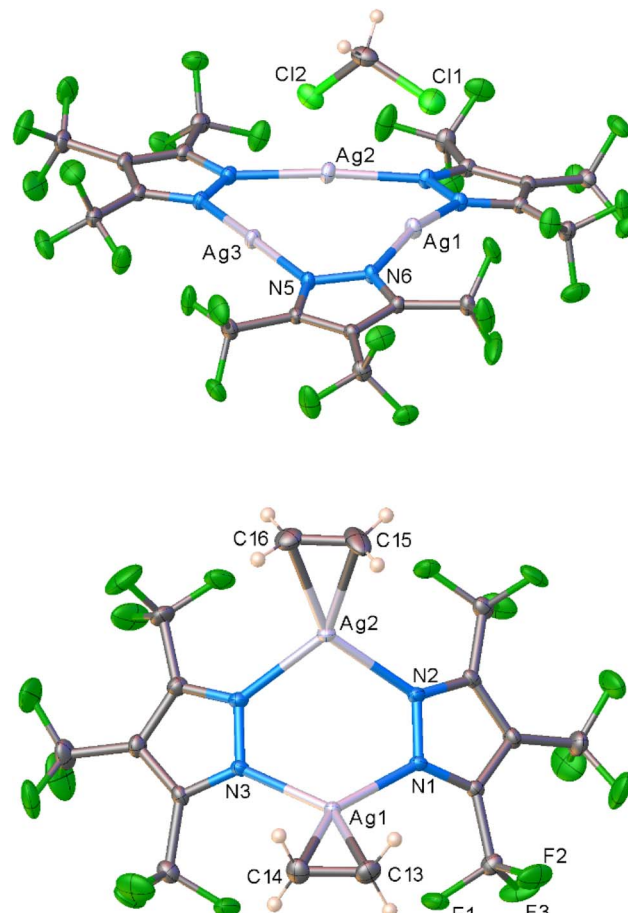


Fig. 2 Molecular structure of $[\text{Ag}-\text{CF}_3]_3 \cdot \text{CH}_2\text{Cl}_2$ (top) and $[\text{Ag}-\text{CF}_3 \cdot (\text{C}_2\text{H}_4)]_2$ (bottom) obtained from solution process and single crystal X-ray diffraction studies.

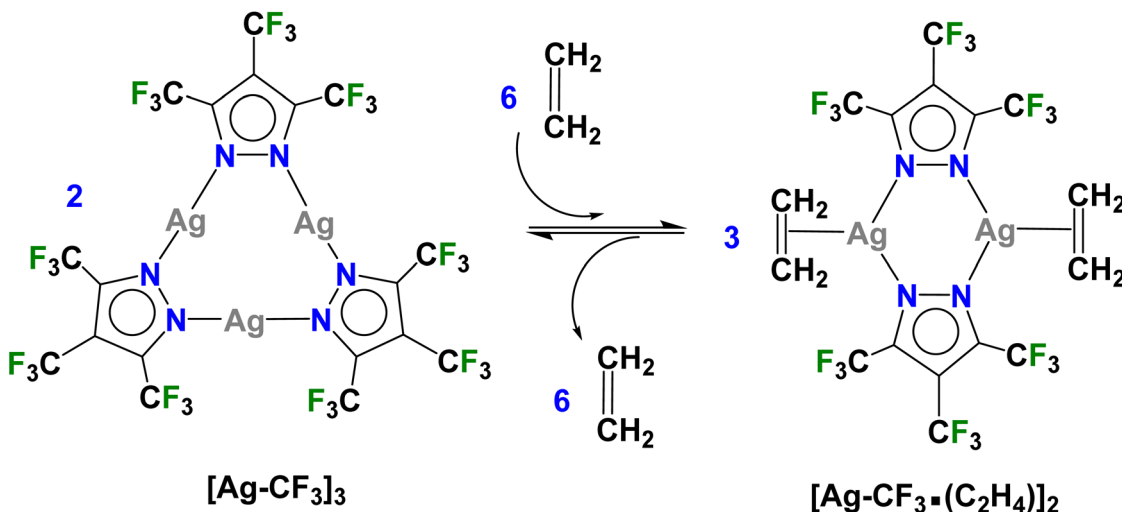
$[\text{CF}_3 \cdot (\text{C}_2\text{H}_4)]_2$ are similar to those observed in $[\text{PhB}(3-(\text{CF}_3)\text{Pz})_3]\text{Ag}(\text{C}_2\text{H}_4)$ (av. Ag–N and Ag–C are 2.261 and 2.264 Å, respectively).

Next, we focussed on the related $\{[3,5-(\text{CF}_3)_2\text{Pz}]\text{Ag}\}_3$ ($[\text{Ag}-\text{H}]_3$),⁹ which is a molecule based on less fluorinated pyrazolate possessing relatively less electrophilic silver sites. Our attempts to observe the silver–ethylene complex from a reaction between $[\text{Ag}-\text{H}]_3$ and ethylene in CH₂Cl₂ solution were unsuccessful even at –50 °C. It is understandable since ethylene–silver bonds in general are quite weak while the Ag–N bonds in $[\text{Ag}-\text{H}]_3$ are relatively strong considering that it features a better electron-donating pyrazolate⁵⁵ than the one present in $[\text{Ag}-\text{CF}_3]_3$.

In situ solid-gas chemistry

We then decided to investigate these processes, using solid materials and study the progress of the reaction “live” using *in situ* PXRD at ANL synchrotron beamline. Recent developments show that *in situ*, *in crystallo*, and solid–gas chemistry are valuable techniques that enable synthesis and characterization of organometallic species that are difficult or impossible to observe under solution-phase conditions.^{30–33} Remarkably, crystals of $[\text{Ag}-\text{CF}_3]_3$ upon exposure to ethylene (3–5 bar at 295





Scheme 1 Ethylene responsive trinuclear silver(I)-pyrazolate $[\text{Ag}-\text{CF}_3]_3$ that undergoes structural changes upon addition of ethylene to form $[\text{Ag}-\text{CF}_3\cdot(\text{C}_2\text{H}_4)]_2$ and reverts to $[\text{Ag}-\text{CF}_3]_3$ upon removal of ethylene.

K, Fig. S10†), converted smoothly to the same dinuclear silver–ethylene complex $[\text{Ag}-\text{CF}_3\cdot(\text{C}_2\text{H}_4)]_2$ (Fig. S13†), mimicking process that occurs in solution. The PXRD based molecular structure of the solid–gas generated $[\text{Ag}-\text{CF}_3\cdot(\text{C}_2\text{H}_4)]_2$ is very similar to that obtained from traditional solution chemistry (and single crystal X-ray crystallography, Fig. 2). It is a reversible process (as in the solution) and affords ethylene free precursor $[\text{Ag}-\text{CF}_3]_3$ (Fig. 3) upon purging crystalline $[\text{Ag}-\text{CF}_3\cdot(\text{C}_2\text{H}_4)]_2$ with helium at 295 K (Fig. S11 and S14†). Furthermore, these solid–gas reactions, despite the complexity and break-up and formation of several bonds and rearrangement of molecular fragments, are quite fast as evident from the PXRD patterns. Although the progress of both the forward and reverse reaction involving $[\text{Ag}-\text{CF}_3]_3$ can be followed using *in situ* PXRD, the trimer–dimer transition under the conditions noted above generates the products directly with no evidence of crystalline phases attributable to intermediates.

To see if we can detect transient species, we proceeded with *in situ* studies of the less reactive $[\text{Ag}-\text{H}]_3$ with ethylene. In contrast to $[\text{Ag}-\text{CF}_3]_3$, the reaction of solid $[\text{Ag}-\text{H}]_3$ with ethylene did not proceed at 295 K even under high ethylene pressure up to 60 bar (ESI Fig. S16†), nor when cooled to 173 K under ~ 1 bar of ethylene flow. However, to our delight, the solid–gas reaction proceeded as we lowered the temperature of polycrystalline $[\text{Ag}-\text{H}]_3$ while subjecting the sample to higher ethylene pressure. Specifically, the transformation was evident from the *in situ* PXRD experiment as the PXRD lines of $[\text{Ag}-\text{H}]_3$ started to disappear around 223 K at 10 bar (or 206 K at 5 bar) of ethylene with the generation of a new crystalline phase (Fig. S17 and S19†). This new phase does not change even upon further cooling to 173 K under ethylene. The process of ethylene uptake by $[\text{Ag}-\text{H}]_3$ is reversible, and the product converts back to ethylene free $[\text{Ag}-\text{H}]_3$ upon warming to about 262 K even under 10 bar of ethylene (Fig. S18†). The PXRD data analysis revealed the structure of the product (illustrated in Scheme 2), which turned out to be not the dinuclear species encountered with $[\text{Ag}-\text{CF}_3]_3$, but an unusual silver–ethylene complex $\{[3,5-(\text{CF}_3)_2\text{Pz}]\text{Ag}(\text{C}_2\text{H}_4)\}_3$ ($[\text{Ag}-\text{H}\cdot(\text{C}_2\text{H}_4)]_3$) that retains the trinuclear form.

The molecular structure of this unprecedented species $[\text{Ag}-\text{H}\cdot(\text{C}_2\text{H}_4)]_3$ is illustrated in Fig. 4 (and S23†). It is a trinuclear silver complex featuring a nine-membered Ag_3N_6 metallacycle, and three trigonal-planar silver–ethylene sites. The Ag_3N_6 core of $[\text{Ag}-\text{H}\cdot(\text{C}_2\text{H}_4)]_3$ displays significant puckering compared to the planar configuration found in $[\text{Ag}-\text{H}]_3$ (and the related $[\text{Ag}-\text{CF}_3]_3$, see Fig. 3).⁹ This large deviation from planarity is a result of the interaction of ethylene with silver sites from opposite faces, but the interactions are perhaps not strong enough to break the Ag–N bonds at low-temperature conditions. The compound $[\text{Ag}-\text{H}\cdot(\text{C}_2\text{H}_4)]_3$ may possibly be a model for a likely intermediate present in more facile reaction of $[\text{Ag}-\text{CF}_3]_3$ with ethylene, just prior to the breakup of trimers to produce the corresponding dinuclear metal–ethylene complexes.

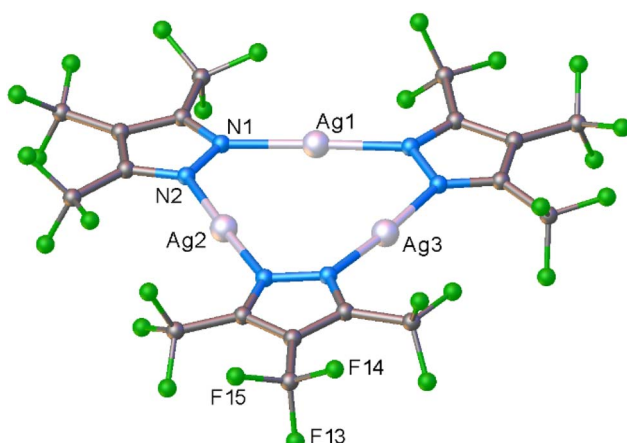
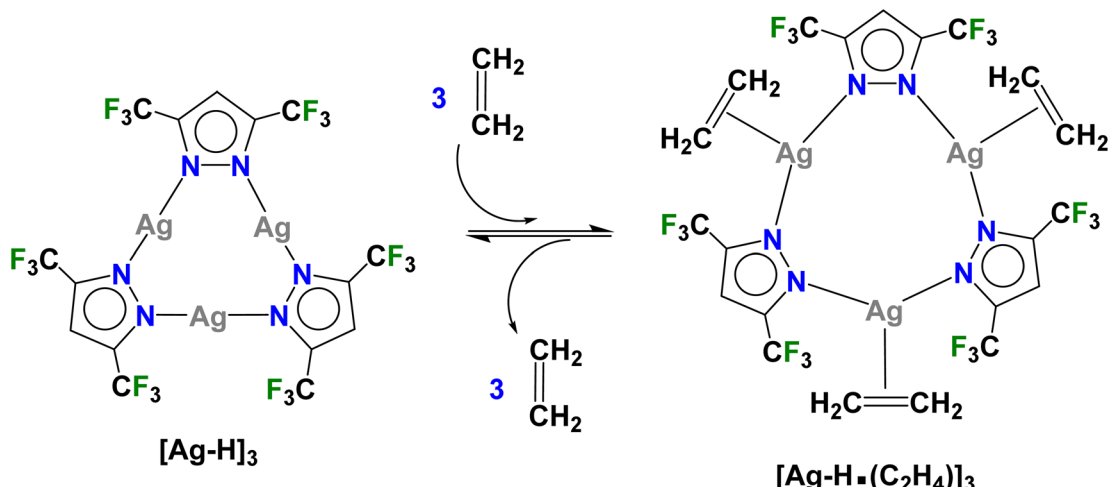


Fig. 3 Molecular structure of $[\text{Ag}-\text{CF}_3]_3$ obtained by *in situ* powder X-ray diffraction studies of the materials from solid–gas chemistry.





Scheme 2 Reaction of $[\text{Ag}-\text{H}]_3$ with 10 bar ethylene below temperature of 223 K (or 5 bar of ethylene below 206 K) leading the trinuclear silver-ethylene complex $\{[3,5-(\text{CF}_3)_2\text{Pz}]\text{Ag}(\text{C}_2\text{H}_4)\}_3$ ($[\text{Ag}-\text{H}\cdot(\text{C}_2\text{H}_4)]_3$) with a nine-membered Ag_3N_6 core.

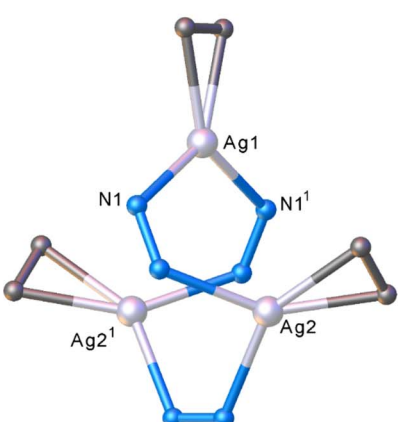
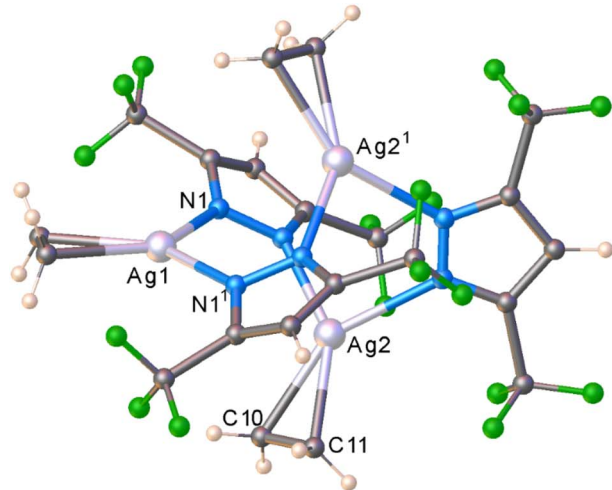


Fig. 4 *In situ* PXRD based molecular structure of the silver-ethylene $[\text{Ag}-\text{H}\cdot(\text{C}_2\text{H}_4)]_3$ complex generated by *in situ* solid-gas chemistry (top). Selected atoms showing only the $\text{Ag}_3\text{N}_6(\text{C}_2\text{H}_4)_3$ moiety and the distorted Ag_3N_6 core (bottom).

Postulating that this ethylene loaded trimer phase $[\text{Ag}-\text{H}\cdot(\text{C}_2\text{H}_4)]_3$ might be a transition state between unloaded trimer and loaded dimer phases observed for other metal pyrazolates, experiments were carried out at even higher pressures and lower temperatures to see if a further transition to a loaded dimer “ $[\text{Ag}-\text{H}\cdot(\text{C}_2\text{H}_4)]_2$ ” could be observed. First, the *in situ* PXRD data were collected at 45 bar of C_2H_4 from room temperature down to 110 K (just above the freezing point of C_2H_4). The pressure was then increased to 70 bar of ethylene and the sample warmed to room temperature (which led to $[\text{Ag}-\text{H}]_3$ formation). We did not observe any evidence of new crystalline phase under both these conditions (see Fig. S25†).

Encouraged by the success with $[\text{Ag}-\text{H}]_3$ that led to the characterization of a rare species in the ethylene bound yet pre trimer \rightarrow dimer transformation stage, we also probed the chemistry of $[\text{Ag}-\text{Br}]_3$ with ethylene. Note that these planar, trinuclear metal adducts display interesting and different extended structures and therefore, the outcome of solid-state chemistry with ethylene is not necessarily predictable through extrapolation. For example, in contrast to $[\text{Ag}-\text{H}]_3$ which crystallizes forming zig-zag columns with argentophilic interactions,^{9,56} $[\text{Ag}-\text{Br}]_3$ trimers form extended structures with inter-trimer $\text{Ag}\cdots\text{Br}$ contacts⁵⁷ (while $[\text{Ag}-\text{CF}_3]_3$ reported here shows inter-trimer $\text{Ag}\cdots\text{F}$ interactions between trimers).

Traditional solution chemistry with ~ 1 bar ethylene thus far did not yield an isolable silver-ethylene complex from $[\text{Ag}-\text{Br}]_3$ in CH_2Cl_2 . The *in situ* PXRD data of the solid-gas reaction of polycrystalline $[\text{Ag}-\text{Br}]_3$ also do not show any phase changes even at 173 K under flow of ethylene (~ 1 bar). However, at 10 bar of ethylene, a notable change was observed at 220 K (Fig. S26†). Data analysis indicated that it directly progressed to the dimer stage producing $\{[4-\text{Br}-3,5-(\text{CF}_3)_2\text{Pz}]\text{Ag}(\text{C}_2\text{H}_4)\}_2$ ($[\text{Ag}-\text{Br}\cdot(\text{C}_2\text{H}_4)]_2$) (Fig. 5 and S30†), which is in contrast to the $[\text{Ag}-\text{H}]_3$ chemistry but similar to that observed with $[\text{Ag}-\text{CF}_3]_3$ and ethylene. Upon warming, $[\text{Ag}-\text{Br}\cdot(\text{C}_2\text{H}_4)]_2$ loses ethylene and returns to the precursor trimer at 295 K, even under 10 bar of ethylene (Fig. S27 and S28†). The dinuclear silver(i)-ethylene complex $[\text{Ag}-$

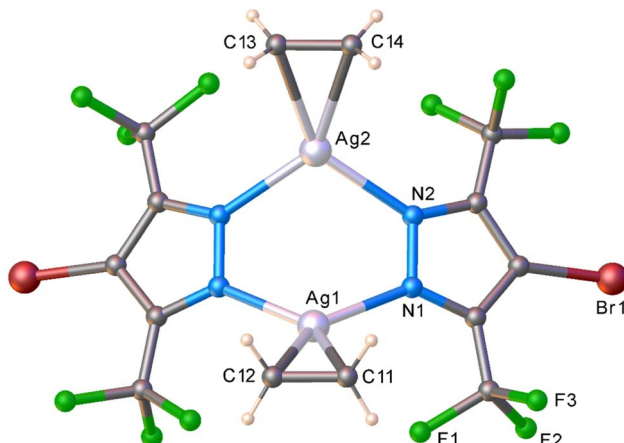


Fig. 5 Molecular structure of *in situ* generated $[\text{Ag-Br}\cdot(\text{C}_2\text{H}_4)]_2$ based on powder X-ray diffraction data.

$\text{Br}\cdot(\text{C}_2\text{H}_4)_2$ adopts a slightly deeper a boat configuration with a closer $\text{Ag}\cdots\text{Ag}$ separation ($3.35(2)$ Å) within the six-membered Ag_2N_4 core relative to that observed with $[\text{Ag-CF}_3\cdot(\text{C}_2\text{H}_4)]_2$ (which has $\text{Ag}\cdots\text{Ag}$ separations at $3.49(2)$ Å). Ethylene ligands are η^2 -bonded to silver sites, as expected. Overall, trinuclear $[\text{Ag-Br}]_3$ and $[\text{Ag-CF}_3]_3$ show unprecedented ethylene triggered solid–gas chemistry leading to dinuclear silver–ethylene complexes featuring Ag_2N_4 cores while $[\text{Ag-H}]_3$ enabled the observation of an ethylene bound silver trimer that retains the metalacyclic Ag_3N_6 core.

Computational study

In order to further understand ethylene driven molecular reorganization processes described above, we undertook a detailed computational study of ethylene reactions of $[\text{Ag-CF}_3]_3$, $[\text{Ag-Br}]_3$ and $[\text{Ag-H}]_3$ (Fig. 6). The Gibbs free energy profiles at 298 K were computed to uncover reaction paths at room temperature in the molecular calculations at the TZ2P/BP86-D3 level of theory. For

this purpose, thermodynamic quantities from vibrational frequencies accounting for enthalpy and entropy changes for the proposed reaction mechanism were obtained (see ESI† for additional details). As the first step (Fig. 6, 1), the formation of an adduct between the trinuclear silver pyrazolate and three molecules of C_2H_4 was predicted, prior to the deformation of the Ag_3N_6 core as a transition state (TS1), which is further relaxed to the intermediate 2 (such as $[\text{Ag-H}\cdot(\text{C}_2\text{H}_4)]_3$). The formation of 2 involves a computed Gibbs free energy (298.15 K) of -16.8 , -15.9 and -13.7 kcal mol $^{-1}$, respectively (Table S10†), in comparison to the initial reactants, for $[\text{Ag-CF}_3]_3$, $[\text{Ag-Br}]_3$ and $[\text{Ag-H}]_3$. The observed deformation of the Ag_3N_6 core from precursors to the intermediates is not favored in the absence of ethylene, by about 50 kcal mol $^{-1}$ (Table S8†) for all the species, showing that such processes is driven exclusively by the initial coordination of C_2H_4 to the bare Ag_3N_6 core (step 1). The process of forming $[\text{Ag-R}\cdot(\text{C}_2\text{H}_4)]_3$ from $[\text{Ag-R}]_3$ and gaseous ethylene ($\text{R} = \text{H, Br, CF}_3$) is not favorable entropically and can be influenced significantly by lower temperatures. Thus, intermediate 2 is more likely to be characterized, especially at lower temperature, as experimentally realized in this work in the reaction involving $[\text{Ag-H}]_3$.

Intermediate 2 is a key step prior to the trimer \rightarrow dimer transformation. After the formation and relaxation of this intermediate, the next step is to release one $[\text{Ag-R}\cdot(\text{C}_2\text{H}_4)]$ unit (*i.e.*, ethylene bound metal-pyrazolate) given as the second transition state (TS2), which is the rate-determinant step leading to the dimer. Calculations of the bonding energy of $\text{Ag}_2\text{N}_4\text{-AgN}_2$ (Table S9†) for $-\text{H}$, $-\text{Br}$ and $-\text{CF}_3$, indicate that it is easier to break-up $[\text{Ag-CF}_3]_3$ and $[\text{Ag-Br}]_3$ species (-64.3 and -65.2 kcal mol $^{-1}$, respectively), in comparison to $[\text{Ag-H}]_3$ counterpart (-83.8 kcal mol $^{-1}$). From the Gibbs free energy profiles (Table S10 and Fig. S31†), the activation barriers related to the $1 \rightarrow \text{TS1}$ process can be evaluated, which amount to 5.0 , 4.7 , and 5.6 kcal mol $^{-1}$ for $-\text{CF}_3$, $-\text{Br}$, and $-\text{H}$ at 298 K, respectively. For the $2 \rightarrow \text{TS2}$ process, the related values are 10.8 , 13.4 , and 14.9 kcal mol $^{-1}$, denoting a slightly larger activation barrier for the $[\text{Ag-H}]_3$ complex.

In the final step, the loss of a $[\text{Ag-R}\cdot(\text{C}_2\text{H}_4)]$ unit from $[\text{Ag-R}\cdot(\text{C}_2\text{H}_4)]_3$, leads to the formation of one dimer species $[\text{Ag-R}\cdot(\text{C}_2\text{H}_4)]_2$ (TS2), where the released unit further aggregates with another $[\text{Ag-R}\cdot(\text{C}_2\text{H}_4)]$ fragment from a parallel reaction, resulting in the formation of a second dimer species (3). Calculated Gibbs free energy for step 3 amounts to -30.1 , -25.5 , and -24.1 kcal mol $^{-1}$ for $[\text{Ag-CF}_3]_3$, $[\text{Ag-Br}]_3$ and $[\text{Ag-H}]_3$, respectively. Overall, $[\text{Ag-H}\cdot(\text{C}_2\text{H}_4)]_2$ formation is slightly less energetically favorable process, while $[\text{Ag-CF}_3\cdot(\text{C}_2\text{H}_4)]_2$ formation is the most facile, which is consistent with the experimental observations, and denoted by the slightly less stabilized transition states and activation barriers, in addition to the bonding energy of $\text{Ag}_2\text{N}_4\text{-AgN}_2$ fragments prior formation of TS2. The formation of trinuclear-tris-ethylene intermediate 2 is favored at lower temperatures but the experimental conditions must be just right to trap this species before it breaks-up to even more energetically favorable dimers 3. The silver(i) and $[3,5\text{-}(\text{CF}_3)_2\text{Pz}]^-$ ligand combination provides the ideal ingredients to trap the elusive species $[\text{Ag-H}\cdot(\text{C}_2\text{H}_4)]_3$.

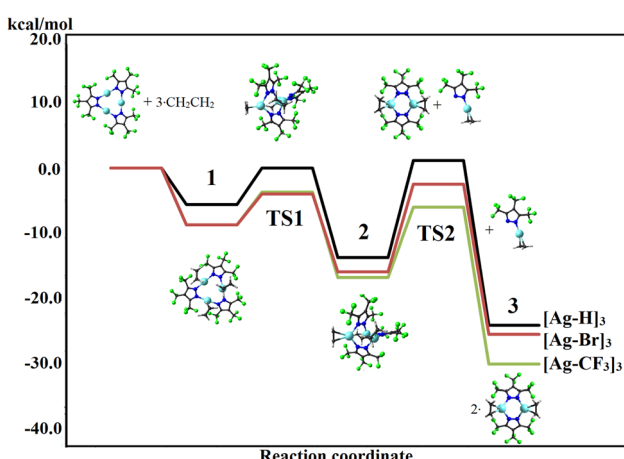


Fig. 6 Gibbs free energy diagram for the proposed mechanism for dimer formation, involving $[\text{Ag-H}]_3$, $[\text{Ag-Br}]_3$, and $[\text{Ag-CF}_3]_3$ at 298 K. Values given per $[\text{Ag-R}]_3$ unit in kcal mol $^{-1}$ ($\text{R} = \text{H, Br, or CF}_3$).



Conclusion

In summary, after a careful investigation that involved strategic variations of pyrazolyl ring substituents and solid-gas synthesis under different temperature-pressure combinations, and synchrotron based, *in situ* PXRD, we successfully trapped and structurally characterized a remarkable, trinuclear silver-ethylene complex $\{[3,5-(CF_3)_2Pz]Ag(C_2H_4)\}_3$ ($[Ag-H \cdot (C_2H_4)]_3$) with a severely distorted, yet intact Ag_3N_6 core, that can be viewed as a model for fleeting intermediates likely exist in ethylene driven, trimer-dimer transformations observed in related $[Ag-CF_3]_3$ and $[Ag-Br]_3$ systems. Furthermore, this study reveals for the first time, ethylene triggered structural transformations of trinuclear silver(i) pyrazolates in the solid-state leading to dinuclear species $\{[3,4,5-(CF_3)_3Pz]Ag(C_2H_4)\}_2$ ($[Ag-CF_3 \cdot (C_2H_4)]_2$) and $\{[4-Br-3,5-(CF_3)_2Pz]Ag(C_2H_4)\}_2$ ($[Ag-Br \cdot (C_2H_4)]_2$), and molecular structures of two rare dinuclear, silver-ethylene complexes. This work also demonstrates the power of *in situ* synthesis and *ab initio* PXRD structure determination over traditional solution chemistry for the isolation and study of labile species. Computational studies indicated that the silver(i) and $[3,5-(CF_3)_2Pz]^-$ ligand combination provides the ideal ingredients to stabilize $[Ag-H \cdot (C_2H_4)]_3$. Further *in situ*, solid-gas studies guided by computational work in search of rare species from other metal complexes are currently underway.

Data availability

All data associated with this article can be found in the ESI.†

Author contributions

Conceived the original idea and project administration (H. V. R. D.), methodology and experimental design (H. V. R. D., A. A. Y., P. W. S., P. M., A. M.-C., E. S.), chemical syntheses, spectroscopy, and data analysis (D. P., M. V., E. S.), DFT calculations and data analysis (A. M.-C.), single and powder XRD and solid-gas synthesis (H. V. R. D., A. A. Y., P. W. S.), writing and proofreading process (all authors).

Conflicts of interest

There are no conflicts to declare.

Acknowledgements

This material is based upon work supported by the National Science Foundation under grant number (CHE-1954456, H. V. R. D.). A. M.-C. thanks the financial support from FONDECYT 1221676. Use of the Advanced Photon Source was supported by the U. S. Department of Energy, Office of Science, Office of Basic Energy Sciences, under contract no. DE-AC02-06CH11357.

References

- 1 J. Zheng, Z. Lu, K. Wu, G.-H. Ning and D. Li, *Chem. Rev.*, 2020, **120**, 9675–9742.
- 2 J. Luo, X. Luo, M. Xie, H.-Z. Li, H. Duan, H.-G. Zhou, R.-J. Wei, G.-H. Ning and D. Li, *Nat. Commun.*, 2022, **13**, 7771.
- 3 R. Galassi, M. A. Rawashdeh-Omary, H. V. R. Dias and M. A. Omary, *Comments Inorg. Chem.*, 2019, **39**, 287–348.
- 4 J.-P. Zhang, Y.-B. Zhang, J.-B. Lin and X.-M. Chen, *Chem. Rev.*, 2012, **112**, 1001–1033.
- 5 J. Zheng, H. Yang, M. Xie and D. Li, *Chem. Commun.*, 2019, **55**, 7134–7146.
- 6 M. A. Omary, M. A. Rawashdeh-Omary, M. W. A. Gonser, O. Elbjeirami, T. Grimes, T. R. Cundari, H. V. K. Diyabalanage, C. S. P. Gamage and H. V. R. Dias, *Inorg. Chem.*, 2005, **44**, 8200–8210.
- 7 A. A. Titov, O. A. Filippov, L. M. Epstein, N. V. Belkova and E. S. Shubina, *Inorg. Chim. Acta*, 2018, **470**, 22–35.
- 8 R. Hahn, F. Bohle, W. Fang, A. Walther, S. Grimme and B. Esser, *J. Am. Chem. Soc.*, 2018, **140**, 17932–17944.
- 9 H. V. R. Dias, S. A. Polach and Z. Wang, *J. Fluorine Chem.*, 2000, **103**, 163–169.
- 10 H. V. R. Dias and C. S. P. Gamage, *Angew. Chem., Int. Ed.*, 2007, **46**, 2192–2194.
- 11 M. A. Rawashdeh-Omary, M. D. Rashdan, S. Dharanipathi, O. Elbjeirami, P. Ramesh and H. V. R. Dias, *Chem. Commun.*, 2011, **47**, 1160–1162.
- 12 M. A. Omary, O. Elbjeirami, C. S. P. Gamage, K. M. Sherman and H. V. R. Dias, *Inorg. Chem.*, 2009, **48**, 1784–1786.
- 13 S.-Z. Zhan, F. Ding, X.-W. Liu, G.-H. Zhang, J. Zheng and D. Li, *Inorg. Chem.*, 2019, **58**, 12516–12520.
- 14 S.-K. Peng, Z. Lu, M. Xie, Y.-L. Huang, D. Luo, J.-N. Wang, X.-W. Zhu, X. Li, X.-P. Zhou and D. Li, *Chem. Commun.*, 2020, **56**, 4789–4792.
- 15 R. Liu, W. Zhang, D. Wei, J.-H. Chen, S. W. Ng and G. Yang, *Dalton Trans.*, 2019, **48**, 16162–16166.
- 16 H. Kestenbaum, A. L. de Oliveira, W. Schmidt, F. Schüth, W. Ehrfeld, K. Gebauer, H. Löwe, T. Richter, D. Lebiedz, I. Untiedt and H. Züchner, *Ind. Eng. Chem. Res.*, 2002, **41**, 710–719.
- 17 J.-X. Liu, S. Lu, S.-B. Ann and S. Linic, *ACS Catal.*, 2023, **13**, 8955–8962.
- 18 R. H. Hertwig, W. Koch, D. Schröder, H. Schwarz, J. Hrušák and P. Schwerdtfeger, *J. Phys. Chem.*, 1996, **100**, 12253–12260.
- 19 H. V. R. Dias and C. J. Lovely, *Chem. Rev.*, 2008, **108**, 3223–3238.
- 20 J. Mehara, B. T. Watson, A. Noonikara-Poyil, A. O. Zacharias, J. Roithová and H. V. R. Dias, *Chem.-Eur. J.*, 2022, **28**, e202103984.
- 21 M. S. Nechaev, V. M. Rayón and G. Frenking, *J. Phys. Chem. A*, 2004, **108**, 3134–3142.
- 22 K. Klimovica, K. Kirschbaum and O. Daugulis, *Organometallics*, 2016, **35**, 2938–2943.
- 23 I. Krossing and A. Reisinger, *Angew. Chem., Int. Ed.*, 2003, **42**, 5725–5728.
- 24 H. V. R. Dias and J. Wu, *Eur. J. Inorg. Chem.*, 2008, 509–522.
- 25 Y. Yin, Z. Zhang, C. Xu, H. Wu, L. Shi, S. Wang, X. Xu, A. Yuan, S. Wang and H. Sun, *ACS Sustainable Chem. Eng.*, 2020, **8**, 823–830.
- 26 R. B. Eldridge, *Ind. Eng. Chem. Res.*, 1993, **32**, 2208–2212.



27 M. G. Cowan, W. M. McDanel, H. H. Funke, Y. Kohno, D. L. Gin and R. D. Noble, *Angew. Chem., Int. Ed.*, 2015, **54**, 5740–5743.

28 D. Parasar, A. H. Elashkar, A. A. Yakovenko, N. B. Jayaratna, B. L. Edwards, S. G. Telfer, H. V. R. Dias and M. G. Cowan, *Angew. Chem., Int. Ed.*, 2020, **59**, 21001–21006.

29 N. B. Jayaratna, M. G. Cowan, D. Parasar, H. H. Funke, J. Reibenspies, P. K. Mykhailiuk, O. Artamonov, R. D. Noble and H. V. R. Dias, *Angew. Chem., Int. Ed.*, 2018, **57**, 16442–16446.

30 K. A. Reid and D. C. Powers, *Chem. Commun.*, 2021, **57**, 4993–5003.

31 F. M. Chadwick, T. Krämer, T. Gutmann, N. H. Rees, A. L. Thompson, A. J. Edwards, G. Bunkowsky, S. A. Macgregor and A. S. Weller, *J. Am. Chem. Soc.*, 2016, **138**, 13369–13378.

32 F. M. Chadwick, A. I. McKay, A. J. Martinez-Martinez, N. H. Rees, T. Krämer, S. A. Macgregor and A. S. Weller, *Chem. Sci.*, 2017, **8**, 6014–6029.

33 J. C. Goodall, M. A. Sajjad, E. A. Thompson, S. J. Page, A. M. Kerrigan, H. T. Jenkins, J. M. Lynam, S. A. Macgregor and A. S. Weller, *Chem. Commun.*, 2023, **59**, 10749–10752.

34 E. Y. Slobodyanyuk, O. S. Artamonov, O. V. Shishkin and P. K. Mykhailiuk, *Eur. J. Org. Chem.*, 2014, 2487–2495.

35 A. A. Mohamed, L. M. Pérez and J. P. Fackler, *Inorg. Chim. Acta*, 2005, **358**, 1657–1662.

36 H. V. R. Dias and H. V. K. Diyabalanage, *Polyhedron*, 2006, **25**, 1655–1661.

37 Y. Morishima, D. J. Young and K. Fujisawa, *Dalton Trans.*, 2014, **43**, 15915–15928.

38 H. V. R. Dias, Z. Wang and W. Jin, *Inorg. Chem.*, 1997, **36**, 6205–6215.

39 H. V. R. Dias and X. Wang, *Dalton Trans.*, 2005, 2985–2987.

40 H. A. Chiong and O. Daugulis, *Organometallics*, 2006, **25**, 4054–4057.

41 H. V. R. Dias, J. Wu, X. Wang and K. Rangan, *Inorg. Chem.*, 2007, **46**, 1960–1962.

42 A. Reisinger, N. Trapp and I. Krossing, *Organometallics*, 2007, **26**, 2096–2105.

43 S. Uchida, R. Kawamoto, H. Tagami, Y. Nakagawa and N. Mizuno, *J. Am. Chem. Soc.*, 2008, **130**, 12370–12376.

44 X. Kou and H. V. R. Dias, *Dalton Trans.*, 2009, 7529–7536.

45 A. Reisinger, N. Trapp, C. Knapp, D. Himmel, F. Breher, H. Rüegger and I. Krossing, *Chem.-Eur. J.*, 2009, **15**, 9505–9520.

46 H. V. R. Dias and J. Wu, *Organometallics*, 2012, **31**, 1511–1517.

47 N. B. Jayaratna, I. I. Gerus, R. V. Mironets, P. K. Mykhailiuk, M. Yousufuddin and H. V. R. Dias, *Inorg. Chem.*, 2013, **52**, 1691–1693.

48 M. Stricker, B. Oelkers, C. P. Rosenau and J. Sundermeyer, *Chem.-Eur. J.*, 2013, **19**, 1042–1057.

49 S. G. Ridlen, J. Wu, N. V. Kulkarni and H. V. R. Dias, *Eur. J. Inorg. Chem.*, 2016, 2573–2580.

50 M. Navarro, J. Miranda-Pizarro, J. J. Moreno, C. Navarro-Gilabert, I. Fernández and J. Campos, *Chem. Commun.*, 2021, **57**, 9280–9283.

51 M. Vanga, A. Muñoz-Castro and H. V. R. Dias, *Dalton Trans.*, 2022, **51**, 1308–1312.

52 B. T. Watson, M. Vanga, A. Noonikara-Poyil, A. Muñoz-Castro and H. V. R. Dias, *Inorg. Chem.*, 2023, **62**, 1636–1648.

53 M. Fianchini, C. F. Campana, B. Chilukuri, T. R. Cundari, V. Petricek and H. V. R. Dias, *Organometallics*, 2013, **32**, 3034–3041.

54 H. V. R. Dias and M. Fianchini, *Angew. Chem., Int. Ed.*, 2007, **46**, 2188–2191.

55 I. I. Gerus, R. X. Mironetz, I. S. Kondratov, A. V. Bezduddy, Y. V. Dmytriv, O. V. Shishkin, V. S. Starova, O. A. Zaporozhets, A. A. Tolmachev and P. K. Mykhailiuk, *J. Org. Chem.*, 2012, **77**, 47–56.

56 H. Schmidbaur and A. Schier, *Angew. Chem., Int. Ed.*, 2015, **54**, 746–784.

57 C. V. Hettiarachchi, M. A. Rawashdeh-Omary, D. Korir, J. Kohistani, M. Yousufuddin and H. V. R. Dias, *Inorg. Chem.*, 2013, **52**, 13576–13583.

